Bulletin of the Seismological Society of America, Vol. 103, No. 1, pp. 157–168, February 2013, doi: 10.1785/0120110313

Low Footwall Accelerations and Variable Surface Rupture Behavior on the Fort Sage Mountains Fault, Northeast California

by Richard W. Briggs, Steven G. Wesnousky, James N. Brune, Matthew D. Purvance,* and Shannon A. Mahan

Abstract The Fort Sage Mountains fault zone is a normal fault in the Walker Lane of the western Basin and Range that produced a small surface rupture (< 20 cm) during an M_L 5.6 earthquake in 1950. We investigate the paleoseismic history of the Fort Sage fault and find evidence for two paleoearthquakes with surface displacements much larger than those observed in 1950. Rupture of the Fort Sage fault ~5.6 ka resulted in surface displacements of at least 0.8–1.5 m, implying earthquake moment magnitudes (M_w) of 6.7–7.1. An older rupture at ~20.5 ka displaced the ground at least 1.5 m, implying an earthquake of M_w 6.8–7.1. A field of precariously balanced rocks (PBRs) is located less than 1 km from the surface-rupture trace of this Holocene-active normal fault. Ground-motion prediction equations (GMPEs) predict peak ground accelerations (PGAs) of 0.2–0.3g for the 1950 rupture and 0.3–0.5g for the ~5.6 ka paleoearthquake one kilometer from the fault-surface trace, yet field tests indicate that the Fort Sage PBRs will be toppled by PGAs between 0.1–0.3g. We discuss the paleoseismic history of the Fort Sage fault in the context of the nearby PBRs, GMPEs, and probabilistic seismic hazard maps for extensional regimes. If the Fort Sage PBRs are older than the mid-Holocene rupture on the Fort Sage fault zone, this implies that current GMPEs may overestimate near-fault footwall ground motions at this site.

Introduction

The Fort Sage Mountains fault zone is located within the northern Walker Lane, a zone of distributed dextral shear that accommodates 10%–15% of the ~50 mm/year of relative plate motion between the Pacific and North American plates (Fig. 1; Thatcher *et al.*, 1999; Hammond and Thatcher, 2007). The Fort Sage fault is a 20-km-long, arcuate normal-oblique fault bound by the strike-slip Warm Springs fault zone on the east and the Honey Lake fault zone on the west (Wills, 1990; also see Data and Resources). The focus of this study is the part of the Fort Sage fault that last ruptured in 1950 during an M_L 5.6 earthquake, producing scarps 12–20 cm high and surface warping of up to 60 cm (Fig. 2; Gianella, 1957).

The surface trace of the 1950 rupture lies within 1 km of a field of previously identified precariously balanced granodiorite boulders (Fig. 3; Brune, 2000, 2003). This study is motivated by the survival of these boulders on the footwall of a historically active fault. In this paper we report the number and timing of paleoseismic ruptures along the Fort Sage fault and discuss the fault rupture history in the context of the nearby precariously balanced rocks (PBRs). We also place our observations in the context of ground-motion prediction equations (GMPEs) for extensional regimes.

Paleoseismic Trench Investigation

We excavated two trenches across scarps on the surface trace of the Fort Sage fault (Fig. 3). The Fort Sage North trench crosses a scarp on an alluvial fan that postdates the 15.7 ka highstand of pluvial Lake Lahontan (Adams and Wesnousky, 1998; Reheis, 1999). The Fort Sage South trench was excavated across a scarp formed on alluvium older than the Lake Lahontan 15.7 ka highstand (Fig. 3) and located directly above the highstand strandline. Both trenches are located along the mapped trace of the 1950 surface rupture (Gianella, 1957; Wills, 1990) and both preserve evidence of pre-1950 surface ruptures.

Fort Sage North Trench

The North trench crosses a 1.6- to 2.1-m-high scarp at the head of a post-Lahontan alluvial fan (Figs. 3 and 4) and exposes loose, fine-grained alluvial grus derived from Cretaceous granodiorite upslope, with two primary depositional

*Also at Seismological Laboratory, University of Nevada, Reno, Reno, Nevada 89557.

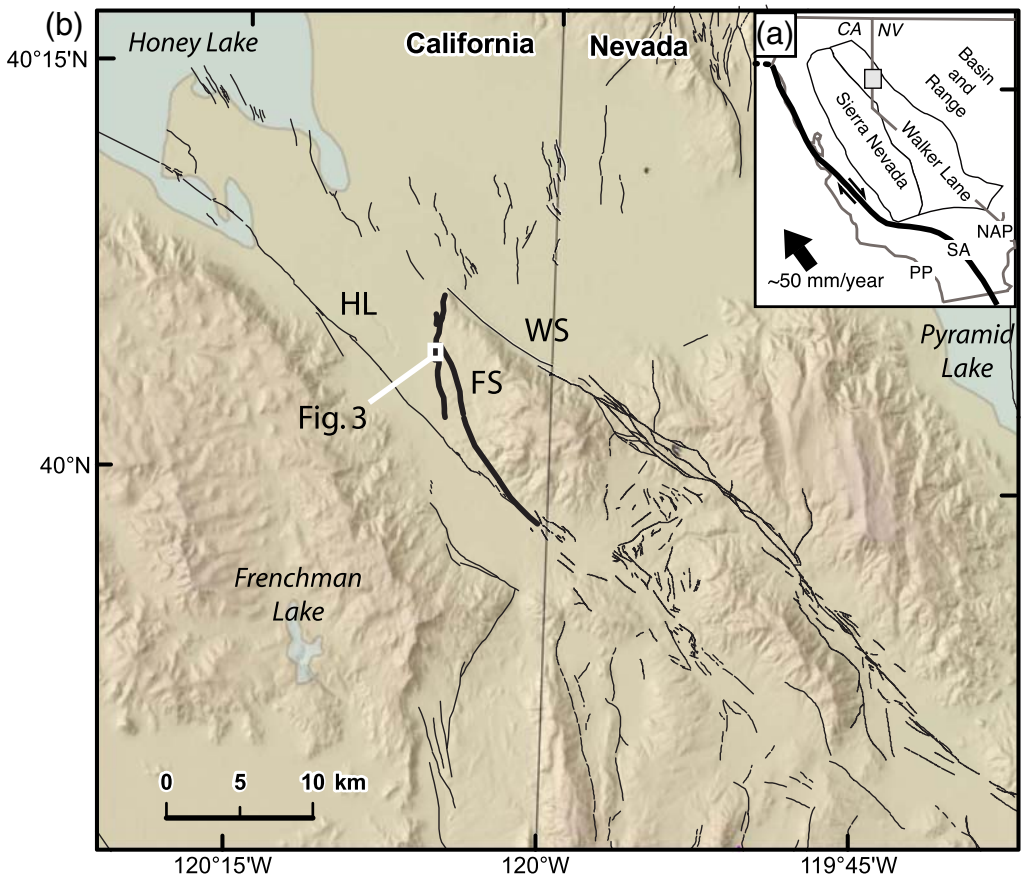

Figure 1. (a) Location of the Walker Lane with respect to the Pacific Plate (PP), San Andreas fault (SA), and North America Plate (NAP). Shaded square indicates extent of Figure 1b. (b) Location of the Fort Sage fault zone (FS). HL, Honey Lake fault zone; WS, Warm Springs fault zone. Faults are from USGS Quaternary Faults-and-Fold Database (see Data and Resources) and base map is generated from Shuttle Radar Topography Mission (SRTM) data (Farr *et al.*, 2007). Shaded areas indicate lakes. The color version of this figure is available only in the electronic edition.

packages (Units 1 and 2) separated by a weak soil (Fig. 4). We observed very little internal stratigraphic structure in the massive grus Units 1 and 2. The scarp-forming fault rupture, event P1, juxtaposes fan stratigraphy in the footwall against a single package of massive scarp-derived colluvium (Unit C1) in the hanging wall. A weak soil (~20 cm of incipient B horizon) is forming at the present-day surface atop colluvial package C1.

The maximum age of event P1 in the North trench can be estimated from detrital charcoal in a weak soil beneath colluvial package C1 (Fig. 4). Sample FSN-C1 (Fig. 4 and Table 1) limits the time of the scarp-forming fault rupture to sometime after 6160 ± 130 cal B.P. (two-sigma 95% errors). The detrital charcoal is likely reworked from wildfires near the site and so this sample is interpreted as providing a maximum limiting age for earthquake P1. The age of sample FSN-C1 is stratigraphically consistent with the slightly older sample FSN-C2 (7165 ± 250 cal B.P.), which was obtained 50 cm lower in the exposure. Optically stimulated luminescence (OSL) ages obtained from the South trench suggest that the maximum age of earthquake P1 may be slightly older than ~6160 ± 130 cal B.P., and OxCal modeling (see Data and Resources and Bronk Ramsey, 2009) of radiocarbon and OSL ages from both trenches suggests an age range of 4.9–6.3 ka for earthquake P1 (see below).

Surface offset from the pre-1950 earthquake P1 at the North trench site can be estimated from the scarp height, the thickness of colluvial package C1, and retrodeformation of the trench units (Fig. 4). The scarp appears to be a single-event feature based on its relatively small size and lack of compound character. The colluvial package C1 is 0.9 m thick and provides a minimum limit on surface displacement and allows a maximum of ~1.8 m, or twice the thickness of the wedge (Fig. 4a). Based on the scarp's topographic profile, the vertical separation across the scarp ranges from 1.6 to 2.1 m depending on whether far-field or near-field surface slopes are projected into the fault zone (Fig. 4b); this projection is complicated by the fan-head setting of the scarp and backtilting of the uphill surface toward the canyon mouth. Retrodeformation suggests that the surface offset was at least 0.9 m, based on restoration of the contact between Units 1 and 2 (Fig. 4c). This reconstruction suggests that Unit 2

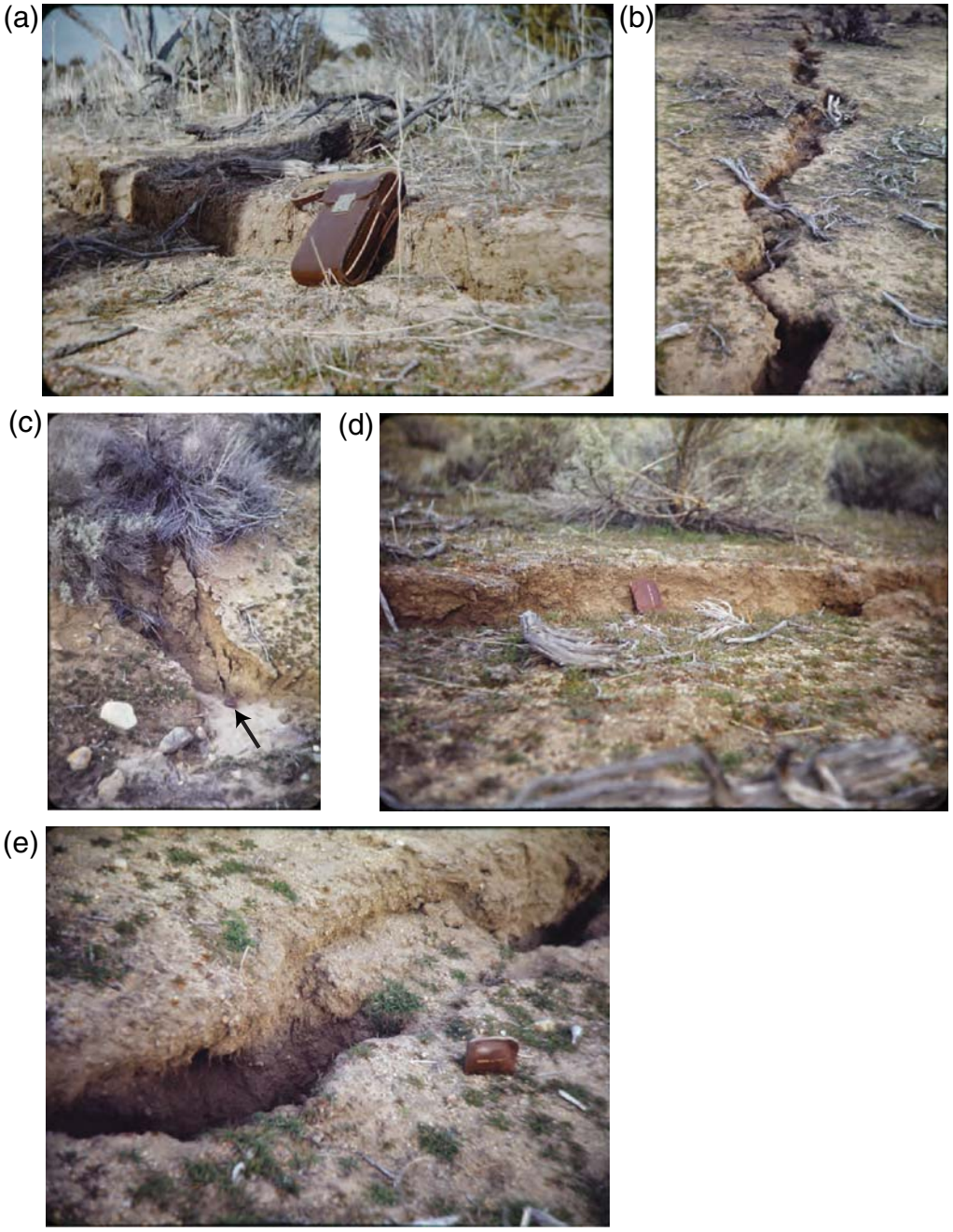

Figure 2. Previously unpublished field photos of the 1950 Fort Sage M_L 5.6 surface rupture. The photos were taken a few days after the earthquake by Ted Ramelli, a rancher from nearby Sierra Valley. Exact locations of photos are unknown. (a) Unweathered scarp in grus. Camera case for scale; estimated long dimension of case is 20 cm. (b) Scarp with associated fissure. No scale; estimated vertical offset is <15 cm. (c) Sharp offset of swale edge, possibly in right-oblique sense. Leather wallet (arrow) is estimated 15 cm long in the longest dimension. (d) Unweathered scarp in grus. Wallet same as previous. (e) Scarp, fissure, and small slump block. Wallet same as previous. The color version of this figure is available only in the electronic edition.

thinned downslope prior to the most recent surface rupture and that the fan deposits possibly draped a preexisting scarp; if this is the case, the scarp height may overestimate fault displacement during event P1. However, a significant component of oblique slip during pre-1950 events (based on observations in the South trench described below) makes reconstructions based only on layer thicknesses suspect. Given these constraints, the most likely surface displacement during the penultimate earthquake P1 is 0.9–1.5 m, which is the minimum offset allowed by scarp-derived colluvium and the smaller estimate of vertical separation across the scarp, minus 12 cm of offset in 1950 at the site reported by Gianella (1957).

We did not recognize the 1950 surface rupture in the North trench exposure, possibly due to the small displacement

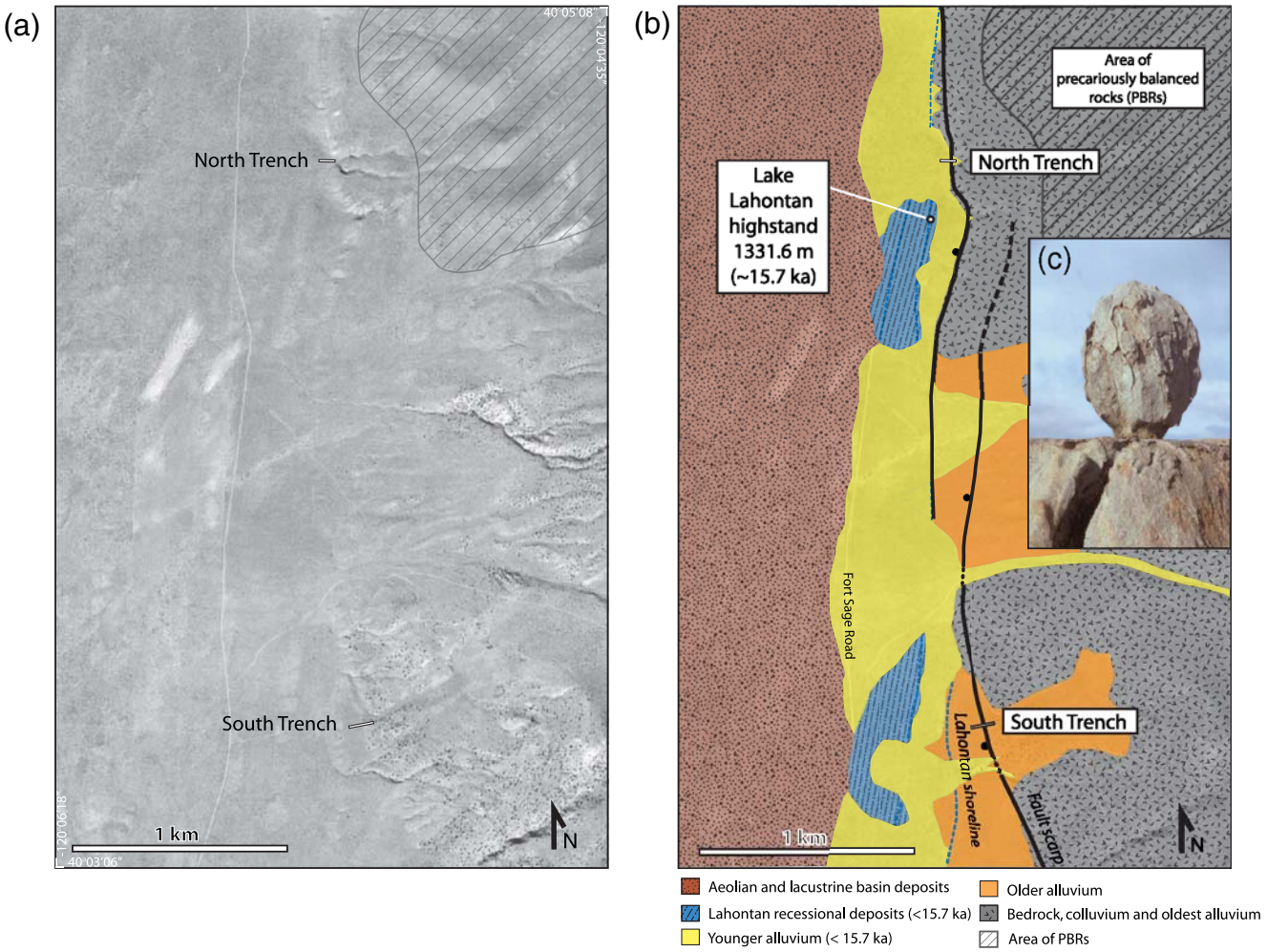

Figure 3. (a) Paired vertical aerial photo and (b) generalized surficial-deposit map showing trench sites with respect to the zone of precariously balanced rocks. (c) Photo of precariously balanced rock is from Brune (2003). Individual rock locations are not shown for their protection and preservation (Anderson *et al.*, 2011). Aerial photo date is 1957. The color version of this figure is available only in the electronic edition.

along this stretch of the fault (approximately 12 cm, as inferred from Gianella, 1957) and relatively poor stratigraphy exposed in the trench. Field photos taken a few days after the 1950 rupture by Ted Ramelli (Fig. 2) show a sharp, decimeter-scale scarp and associated fissure. The granite grus of the fan surface is easily weathered, and Gianella (1957) reported "(I)n June, 1956… little evidence of the (1950 scarps) remain." Rapid scarp degradation after 1950 is also evident in the 1958 field photos of Karl Steinbrugge, which show only discontinuous, low-angle scarps that are "the best remaining examples of faulting in this area" (see Data and Resources). No obvious surface expression of the 1950 earthquake remains along the Fort Sage rangefront today.

Fort Sage South Trench

The South trench crosses an approximately 2.0-m-high scarp on an alluvial fan just above the 15.7 ka highstand of Lake Lahontan (Figs. 3 and 5). The trench exposes well-sorted fluvial sands and gravels (Units 1a–d) and poorly sorted debris-flow deposits (Units 2a–c) derived from conglomerates, sandstones, and granodiorites upslope (Fig. 5). These units are vertically offset by a main fault zone *a* and subsidiary fault zones *b*–*f*, resulting in the formation and preservation of colluvial packages C1 and C2.

The 1950 rupture is expressed in the South trench as the extension of shear zones to the surface and as a thickened Av soil horizon (approximately 5 cm) between the main fault zone *a* and secondary fault zone *b* (Fig 5). Aside from this zone of thickened silt, we did not observe a colluvial package associated with the small 1950 rupture here, and deformation appears to have occurred mainly in the form of warping and cracking as discussed by Gianella (1957).

Stratigraphic evidence shows that two surface-rupturing earthquakes, events P1 and P2, occurred at this site prior to the 1950 rupture (Fig. 5). The most recent pre-1950 earthquake, event P1, is indicated by the scarp-derived colluvial package C1 and by a fissure in underlying colluvial package

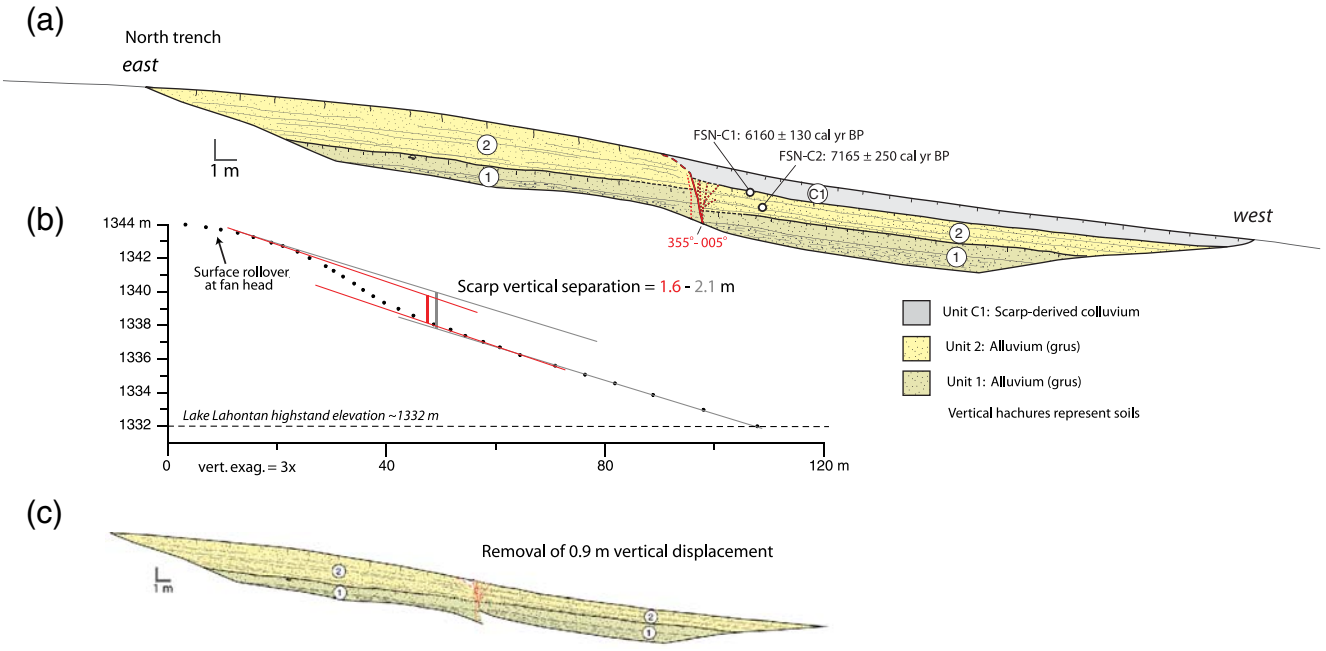

Figure 4. (a) Log of Fort Sage North trench exposure. Units 1 and 2 are weakly bedded grus separated by an incipient soil, and C1 is scarp-derived colluvium. Fault zone and fault strike are shown in red. (b) Estimates of vertical separation across scarp. Range is due to variable far-field projection of surfaces into the fault zone. (c) Restoration of 0.9 m of vertical displacement removes colluvium C1 and aligns the contact between Units 1 and 2. The color version of this figure is available only in the electronic edition.

C2 that is filled with Unit C1. We correlate colluvial packages C1 in both the North and South trenches on the basis of their similar stratigraphic positions, thicknesses, close proximity of trenches, and soil development (~20 cm of incipient B horizon development at the modern surface). Vertical offset during event P1 in the South trench is at least 0.8 m, or the maximum thickness of the C1 colluvium.

Evidence for the second paleoearthquake in the South trench, paleoearthquake P2, is preservation of the scarp-derived colluvial package C2. A period of prolonged surface stability following this event resulted in the formation of a weak argillic B horizon on colluvium C2 and a well defined stone line. This buried soil and prominent stone line allow easy differentiation between colluvial packages C1 and C2. The vertical offset from event P2 was at least 1.5 m based on the maximum thickness of colluvial package C2.

Age control for events P1 and P2 in the South trench is from OSL on quartz grains and infrared stimulated luminescence (IRSL) on feldspar grains. These dates are from bulk samples of fine-grained sediment (Fig. 5 and Table 2). The age of paleoearthquake P1 is constrained by samples FSS-OSL-1 and -2, which limit the time of P1 in the South trench to between 7.76 ± 1.12 ka and 17.9 ± 2.66 ka (two-sigma [95%] errors). This interval is slightly older than, and does not overlap with, the 6.1 ± 0.13 ka maximum age for paleoearthquake P1 obtained from the North trench. The OSL age from post-paleoearthquake P1 colluvium (C1) in the South trench (7.76 ± 1.12 ka) is slightly older than the radiocarbon date for the pre-earthquake buried surface in the North trench (6.1 ± 0.13 ka). The older, higher date may result from incomplete resetting of sample FSS-OSL-1. Paleoearthquake P2 occurred between 17.9 ± 2.24 and

Table 1
Radiocarbon Ages from Fort Sage North Trench

Sample Name	CAMS Number*	$d^{13}C^{\dagger}$	Fraction Modern	±	$D^{14}C$	±	^{14}C age (Year)‡	±2 s	Cal BP§	±2 s
FSN-C1	121670	−25	0.5107	0.0020	−489.3	2.0	5400	35	6160	130
FSN-C2	121671	−25	0.4593	0.0052	−540.7	5.2	6250	100	7165	250

*Samples analyzed at the Center for Accelerator Mass Spectrometry, Lawrence Livermore National Laboratory Laboratory.

†$d^{13}C$ values are the assumed values according to Stuiver and Polach (1977) when given without decimal places. Values measured for the material itself are given with a single decimal place.

‡The quoted age is in radiocarbon years using the Libby half-life (5568 years) following the conventions of Stuiver and Polach (1977).

§Calibrations are performed with the IntCal09 calibration curve (Reimer *et al.*, 2009) and OxCal version 4.1 (Bronk Ramsey, 2009).

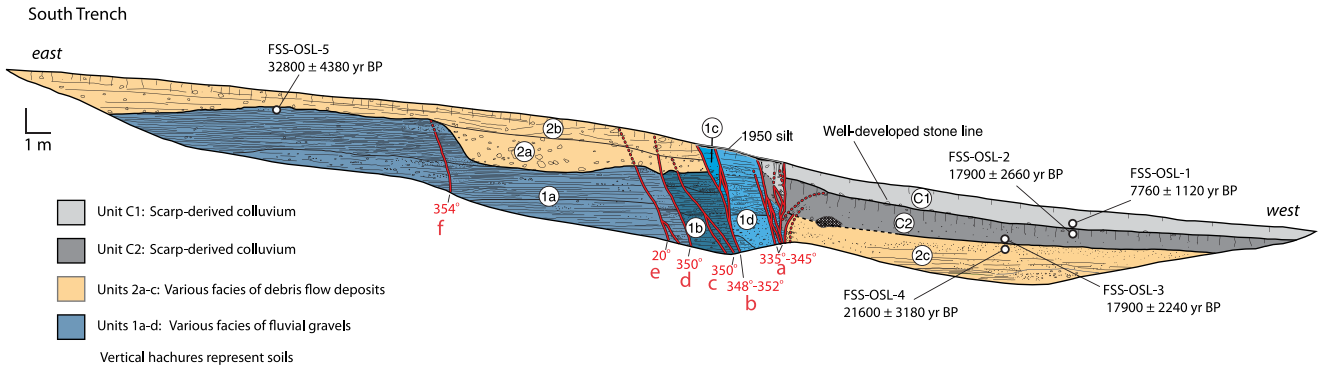

Figure 5. Log of Fort Sage South trench exposure. Units 1a–d are well-sorted fluvial sands and gravels; Units 2a–c are poorly sorted debris flow deposits; and C1 and C2 are scarp-derived colluvium. Subvertical faults are shown with their strikes. The color version of this figure is available only in the electronic edition.

21.6 ± 3.18 ka based on bounding samples FSS-OSL-3 and -4. Events P1 and P2 are both younger than 32.8 ± 4.38 ka, which is the minimum age of footwall deposits estimated from sample FSS-OSL-5.

To better constrain the ages of paleoearthquakes P1 and P2 with dates from both trenches, we model their probable age ranges using the program OxCal (Fig. 6; see Data and Resources), which uses Bayesian statistics and stratigraphic ordering information to create probability distributions for boundaries between ordered, and often overlapping, dates (Lienkaemper and Bronk Ramsey, 2009). The assumptions of the model we developed in OxCal (see Appendix) are: (1) paleoearthquake P1 is the same event in both trenches; (2) earthquakes are best modeled as boundaries in OxCal; and (3) OSL dates FSS-OSL-2 and -3 from the South trench are best combined to form a phase within the model, although combining these dates has very little effect on the model results.

The main outcome of the OxCal modeling is that the most likely age of paleoearthquake P1 is 5.6 ± 0.7 ka (6275–4923 BP; two-sigma [95%] confidence interval; Fig. 6). This interval includes the age range for an earthquake that occurred after 6.1 ± 0.13 ka (radiocarbon sample FSN-C1; North trench) but before the (apparently inverted) overlying OSL age of 7.76 ± 1.12 (FSS-OSL-1; South trench). Because the age of sample FSS-OSL-1 (South trench) is inverted with respect to the underlying radiocarbon ages of samples FSN-C1 and -C2 (North trench), the OxCal model returns a poor agreement index A value (19.9%) for the modeled age of the sample FSS-OSL-1 (6195–4220 BP). This is a formal indication that sample FSS-OSL-1 is an outlier. Alternatively, the underlying radiocarbon ages FSN-C-1 and FSN-C-2 may be too young if they were not obtained from detrital charcoal emplaced in successive debris-flow deposits as interpreted from the trench exposure. In any case, the combined OSL and radiocarbon dates and stratigraphic evidence point toward a large surface-rupture earthquake at ~5.6 ka in both trenches.

The age of paleoearthquake P2 obtained from the OxCal model is 20.5 ± 5.2 ka, similar to but slightly older than the ~19.8 ka age of P2 interpreted from OSL bounding ages in the South trench alone. While a robust recurrence interval cannot be obtained from only two events, it appears that the Fort Sage fault ruptures in large ($>M$ 6.8) earthquakes

Table 2
Quartz OSL and Feldspar IRSL Ages from Fort Sage South Trench

Sample Name	% Water Content*	K (%)†	U (ppm)†	Th (ppm)†	Cosmic Dose‡ Additions (Gy/ka)	Total Dose Rate (Gy/ka)	Equivalent Dose (Gy)	n§	Age (ka)¶
FSS-OSL-1	1 (27)	2.30 ± 0.08	2.41 ± 0.15	11.2 ± 0.29	0.12 ± 0.01	3.71 ± 0.07	28.8 ± 2.02	22 (30)	7.76 ± 1.12
FSS-OSL-2	1 (27)	1.93 ± 0.12	2.45 ± 0.13	12.0 ± 0.30	0.09 ± 0.01	3.29 ± 0.07	58.9 ± 4.12	18 (20)	17.9 ± 2.66
FSS-OSL-3	1 (28)	1.98 ± 0.12	2.59 ± 0.11	12.0 ± 0.30	0.04 ± 0.004	3.32 ± 0.07	59.3 ± 3.50	20 (25)	17.9 ± 2.24
FSS-OSL-4	1 (28)	2.18 ± 0.12	2.25 ± 0.13	10.2 ± 0.31	0.03 ± 0.003	3.29 ± 0.07	71.1 ± 5.03	17 (25)	21.6 ± 3.18
FSS-OSL-5	1 (34)	2.05 ± 0.13	2.39 ± 0.14	12.5 ± 0.26	0.12 ± 0.01	3.38 ± 0.06	111 ± 7.22	31 (35)	32.8 ± 4.38

*Field moisture, with figures in parentheses indicating the complete sample saturation %. Ages calculated at 15% of complete saturation for Holocene, 25% saturation for Pleistocene.

†Analyses obtained using laboratory Gamma Spectrometry (low resolution NaI detector).

‡Cosmic doses and attenuation with depth were calculated using the methods of Prescott and Hutton (1994).

§Number of replicated equivalent dose (De) estimates used to calculate the mean Figures in parentheses indicate total number of measurements made including failed runs with unusable data.

¶Dose rate and age for fine-grained 250–180 μm quartz sand. Linear and exponential fit used on age, errors to two sigma.

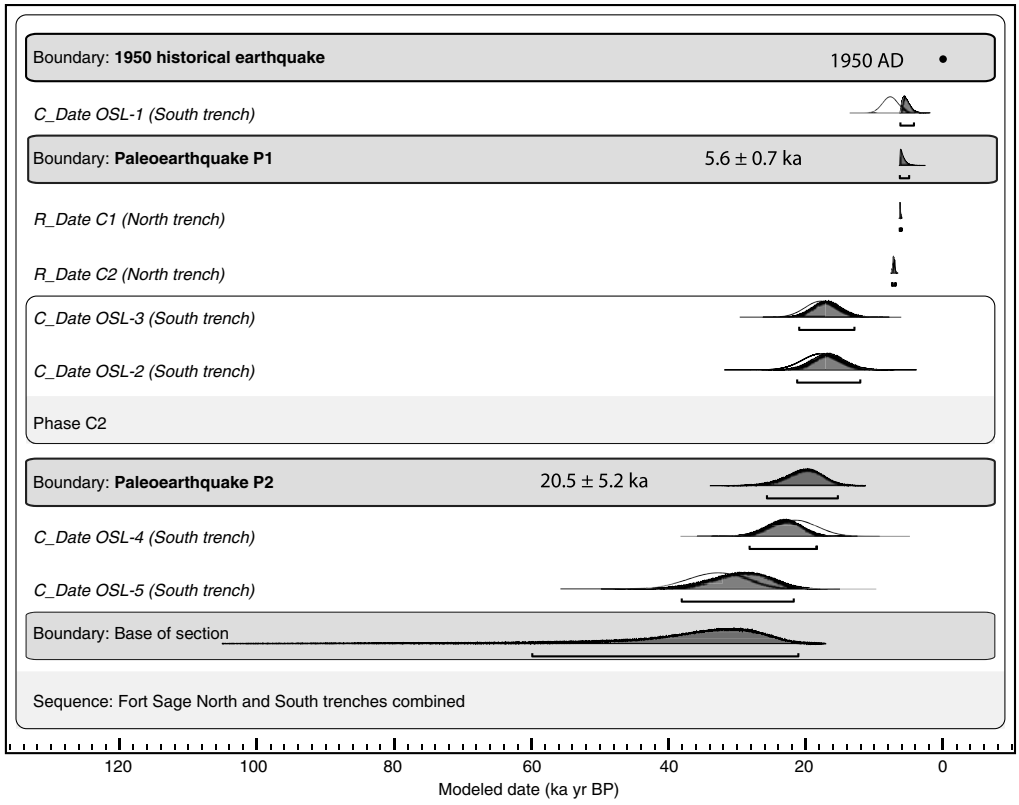

Figure 6. OxCal model of a sequence that combines North and South trench dates in a composite stratigraphy. Dates are shown as probability distribution functions (PDFs). Light grey distributions are the likelihood distributions of the OSL and radiocarbon dates, and darker distributions are modeled (posterior) PDFs. Bars below PDFs show the 95-percentile confidence ranges. Paleoearthquakes P1 and P2 are modeled as boundaries.

at time scales of approximately 10–20 ka, similar to recurrence intervals obtained for typical Basin and Range normal faults (Wesnousky *et al.*, 2005).

The footwall deposits east of the main fault zone in the South trench are deformed by several subsidiary shear zones *b*–*f*, and the stratigraphic packages they juxtapose are denoted as Units 1a–d on Figure 5. Pronounced changes in layer thicknesses, facies mismatches, and apparent reverse displacement across these footwall shears suggest a substantial oblique component of deformation. The strike of the subsidiary faults is rotated 10°–40° in a clockwise direction with respect to the main fault zone, suggesting that they are R-type shears resulting from right-oblique offset (Fig. 5). The facies mismatch between the debris-flow deposits of the hanging wall (Unit 2c) and the uppermost footwall (Unit 2b) may also be evidence of oblique offset. However, no correlative laterally offset features were observed in the trench exposure. Shears that terminate in the footwall block, such as strands *c* and *f*, are probably evidence of older, undated events in the exposure.

Predicted Paleoearthquake Magnitudes

The moment magnitude (M_w) of an earthquake can be estimated from regressions that relate displacement to magnitude. Given that we only have displacement values obtained directly from trench exposures, we use these data to estimate paleoearthquake magnitude because independent limits on paleorupture length or area are not available. The trenches record vertical displacements from paleoearthquake P1 of 0.8–1.5 m, which correspond to M_w 6.9–7.1 using the regression of Wells and Coppersmith (1994), or M_w 6.8–7.1 using the approach of Biasi and Weldon (2006).

The regressions of Wells and Coppersmith (1994) and Biasi and Weldon (2006) use mean displacement values. It is difficult to obtain mean event displacements from our trenches because we have only two closely spaced sites along the fault, but if we take 1.15 m to represent mean offset during paleoearthquake P1 (the value midway between 0.8 and 1.5 m), both the Wells and Coppersmith (1994) and Biasi and Weldon (2006) methods predict a paleoearthquake magnitude of M_w 7.0. The full range of paleoearthquake magnitudes that might accompany 1.15 m of average surface offset, given that we have only two measurements that span less than 10% of the length of the fault, is M_w 6.7–7.9 (Hemphill-Haley and Weldon, 1999). The largest value, M_w 7.9, seems highly unlikely given that the mapped length of the Fort Sage fault zone is only about 20 km. Given the uncertainties in our displacement measurements and the

displacement-to-magnitude regressions, we use M_w 6.7–7.1 as the most likely size of paleoearthquake P1.

A similar exercise for paleoearthquake P2 using the minimum displacement value of 1.5 m observed in the South trench leads to a paleoearthquake estimate of M_w 7.1 and a possible range of M_w 6.8–8.0. Using logic similar to above, we use M_w 6.8–7.1 as the most likely size of paleoearthquake P2.

Fort Sage Precarious Boulder Field

The surface trace of the Fort Sage fault is less than 1 km from a field of precariously balanced rocks, or PBRs (Fig. 3; Brune, 2000; Anderson *et al.*, 2011). PBRs are rocks balanced on pedestals and that have high height-to-width ratios making them easily susceptible to toppling (Fig. 3c; Brune, 1996). PBRs on granitic tors such as the Fort Sage Mountains are formed by chemical weathering and subsequent physical exhumation of relatively resistant corestones (Linton, 1955).

Precariously balanced rocks are natural ground-motion instruments (Brune, 1996), and numerous field and theoretical studies have demonstrated that untoppled PBRs place limits on ground motions near active faults (Brune, 1996; Shi *et al.*, 1996; Anooshehpoor and Brune, 2002; Brune *et al.*, 2006). PBRs potentially record paleo-ground motions in regions with few instrumental records and PBR-derived ground-motion information may be of value in probabilistic seismic hazard analyses (PSHA) (Anderson and Brune, 1999; Stirling *et al.*, 2002; O'Connell, LaForge, and Liu, 2007; Purvance *et al.*, 2008; Anderson *et al.*, 2011).

Because the Fort Sage PBRs are very near the surface trace of an active normal fault, they present an opportunity to place limits on near-field, normal-fault, footwall ground motions (Brune, 2000). Theoretical studies predict that ground motions are asymmetric about dipping faults that juxtapose dissimilar material (Shi *et al.*, 1997; Oglesby *et al.*, 1998; Brune and Anooshehpoor, 1999; O'Connell, Ma, and Archuleta, 2007; Ma and Beroza, 2008). Instrumental strong-motion records near the surface trace of a normal-fault earthquake are rare, with one exception being the observation that peak accelerations were nearly 50% lower on the footwall than on the hanging wall during the 2006 M_w 5.4 Morelia, Mexico, normal-fault earthquake (Munguía *et al.*, 2009).

Quasi-static toppling tests of the Fort Sage PBRs show that they can be toppled by horizontal accelerations of 0.2g, with a range of toppling accelerations of 0.1–0.3g (Brune, 2000; M. D. Purvance, unpublished data, 2011). The age of the Fort Sage PBRs is unknown. By analogy with similar PBRs in southern California that have been dated with cosmogenic surface exposure techniques (Bell *et al.*, 1998; Balco *et al.*, 2011), the Fort Sage PBRs are probably over 10,000 years old. Post-Lahontan (15.7 ka) erosion rates determined by cosmogenic nuclide analysis in the Fort Sage Mountains along catchment margins are 2–3 cm/ka (Granger *et al.*, 1996; Riebe *et al.*, 2000), making it unlikely that entire several-meter-high boulders and their pedestals have been exhumed since desiccation of Lake Lahontan. We estimate ages of 10 ± 5 ka for the Fort Sage PBRs in their present unstable form on the basis of present-day erosion rates and analogs in southern Nevada and California (Bell *et al.*, 1998; Balco *et al.*, 2011). Determination of the actual ages of Fort Sage PBRs will require a focused cosmogenic nuclide dating and modeling effort as recently demonstrated by Balco *et al.* (2011). While we consider it unlikely, the possibility that the Fort Sage PBRs represent a statistical remnant of a former larger population of toppled rocks (O'Connell, LaForge, and Liu, 2007) should be addressed by a detailed mapping effort.

Predicted Peak Ground Acceleration

Predictions of peak ground acceleration (PGA) are derived from models that estimate ground motions based on earthquake magnitudes, site conditions, faulting style, and attenuation relations. Several ground-motion prediction equations have been developed for extensional regions and normal faults (Power *et al.*, 2008). We apply a representative sample of GMPEs (Spudich *et al.*, 1999; Pankow and Pechmann, 2004; Abrahamson and Silva, 2008; Boore and Atkinson, 2008; Campbell and Bozorgnia, 2008; Chiou and Youngs, 2008) to the 1950 M_L 5.6 surface-rupture earthquake and to the range of paleoearthquake magnitudes (M_w 6.7–7.1) that we calculate from fault offsets associated with paleoearthquake P1. For all models we calculate PGA at a hard-rock site ($V_{S30} = 760$ m/s) on the fault footwall and assume a 45°-dipping fault plane. We calculated distance with respect to the surface-rupture trace. Calculations were performed using Open SHA, an open-source platform for conducting seismic hazard analysis (Field *et al.*, 2003; also see Data and Resources).

For the 1950 M_L 5.6 surface-rupture earthquake, the GMPEs predict median PGAs ranging from 0.2 to 0.3g at 1 km, the distance from the 1950 surface-rupture trace to the nearby PBR field (Fig. 7a). The Abrahamson and Silva (2008), Campbell and Bozorgnia (2008), and Chiou and Youngs (2008) GMPEs predict median PGAs of 0.3g and above, sufficient to topple most of the Fort Sage PBRs. The Spudich *et al.* (1999) and Boore and Atkinson (2008) GMPEs predict median PGAs of 0.20–0.22, very near the 0.2g toppling value for the Fort Sage PBRs derived from field tests. No field survey of the Fort Sage PBRs was conducted after the 1950 earthquake, but reconnaissance inspection of the Fort Sage PBR field does not show evidence for boulders toppled in 1950. This observation suggests that the existing suite of GMPEs overpredicts near-fault footwall ground motions for this small-magnitude earthquake. A direct test of this hypothesis will require careful mapping of the Fort Sage PBR field.

For paleoearthquake P1 of estimated magnitude 6.7–7.1, the GMPEs predict PGAs ranging from 0.3 to 0.5g at 1 km (Fig. 7b). The variation in the predicted ground motions arises from differing assumptions built into the models. Nonetheless,

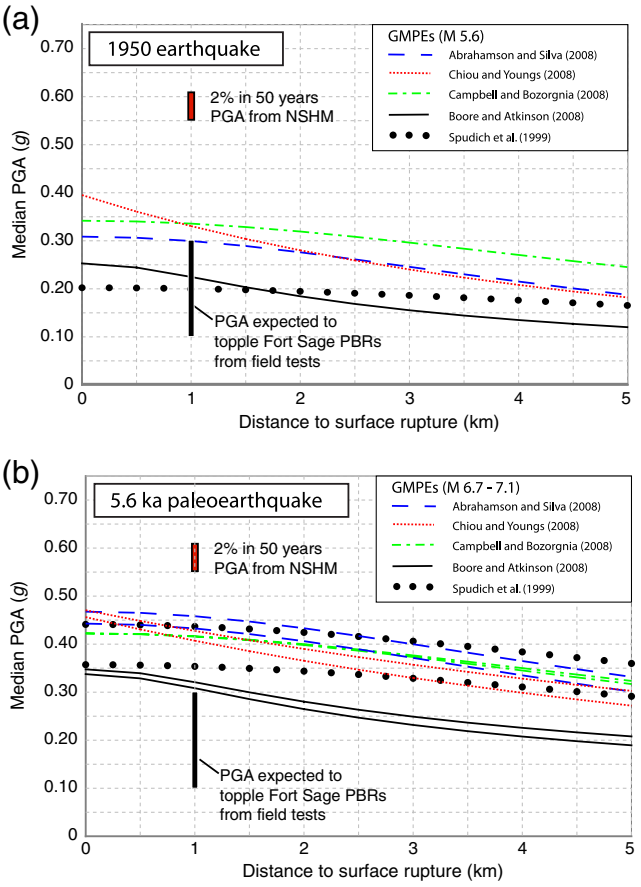

Figure 7. Median PGA (g) plotted against distance from the surface trace of the Fort Sage fault from ground-motion prediction equations (GMPEs). (a) Ground-motion predictions for the 1950 M_L 5.6 surface-rupture earthquake. The Fort Sage PBRs are < 1 km from the fault. PGA expected to topple Fort Sage PBRs is from Brune (2000). Two percent in 50 years PGA at PBR site is from the 2008 update of the National Seismic Hazard Maps (Petersen *et al.*, 2008). Calculations performed with Open SHA (Field *et al.*, 2003). (b) Ground-motion predictions for paleoearthquake P1 at ~5.6 ka, which is inferred to have ranged in magnitude from M_w 6.7–7.1. The color version of this figure is available only in the electronic edition.

they all predict peak accelerations for the Fort Sage boulder field that are larger than the toppling accelerations derived from field measurements. The model of Boore and Atkinson (2008) predicts the lowest ground motions at all distances from the fault, but still predicts slightly higher accelerations ($0.3g$) than would be required to topple most of the Fort Sage PBRs.

The U.S. Geological Survey National Seismic Hazard Map (NSHM) depicts accelerations as the sum of probabilities of all potential sources that contribute to ground motion at a site (Petersen *et al.*, 2008). At the location of the Fort Sage PBRs, the 2008 update of the NSHM estimates a PGA of $0.55–0.61g$ at the 2%-in-50 years level (~2475 year return time), a typical return time used for building design in low-seismicity regions of the conterminous United States (Fig. 7). The NSHM does not provide site-specific hazard curves, but the hard-rock site conditions (granitic bedrock) at the location of the Fort Sage PBRs (Kalkan *et al.*, 2010) are an appropriate application of the generic NSHM curves, which are calculated for V_{S30} = 760 m/s. Thus an important inference derived from the National Seismic Hazard Maps is that the PBRs at Fort Sage have been subject to ~0.6 PGA (2% in 50 years, or 2475-year return time) shaking at least twice due to all regional sources since ~5 ka.

Summary and Conclusions

Rupture of the Fort Sage fault between 4.9–6.3 ka resulted in surface displacements of at least 0.8–1.5 m, implying a paleoearthquake of M_w 6.7–7.1. Based on a suite of commonly employed ground-motion prediction equations, the predicted range of footwall PGAs at 1 km distance from the surface paleorupture during this paleoearthquake is $0.3–0.5g$.

Precariously balanced rocks that can be toppled by accelerations of $0.1–0.3g$ are located less than 1 km from the Fort Sage fault-surface trace. The age of these rocks is unknown, but we estimate that they gained their currently unstable form at 10 ± 5 ka. If these PBRs are older than 4.9–6.3 ka (which is very likely), then they have survived at least one M_w 6.7–7.1 earthquake on a normal fault less than 1 km away. The presence of the Fort Sage PBRs argues for low PGAs at the site despite their close proximity to three Holocene-active faults (the Honey Lake, Warm Springs, and Fort Sage faults). Furthermore, survival of these rocks contrasts with the higher accelerations predicted deterministically by commonly used GMPEs and the probabilistic predictions of the NSHM.

There are at least three explanations for the apparent discrepancy between a large surface-rupture mid-Holocene earthquake on the Fort Sage fault and the presence of a PBR field less than 1 km away. First, our paleoseismic results may be flawed and paleoearthquake P1 may be incorrectly dated, or the paleoearthquake magnitude may be overestimated. We consider this unlikely because the 4.9–6.3 ka age of event P1 is well constrained by straightforward geomorphology and stratigraphy at two trenches with radiocarbon and OSL ages, and the vertical surface offsets observed in both trenches (0.8–1.5 m) are consistent with a large (M_w 6.7–7.1) earthquake. A second explanation may be that the assumed ages (10 ± 5 ka) and fragility (toppling at 0.1–0.3 PGA) of the PBRs might be incorrect. Third, the GMPEs commonly used for normal faults might not fully capture near-fault ground motions, or they may overestimate accelerations overall. To explain the apparent discrepancy between the paleoseismic information, PBR observations, and GMPEs, we recommend that the ages and fragilities of the Fort Sage PBRs be conclusively established and that the GMPEs be reevaluated in the context of the geologic field data.

An important result of this work for paleoseismic trenching studies is that evidence of the 1950 rupture is absent or obscure, which highlights the problem of recognizing small-offset earthquakes in relatively coarse-grained deposits. Because of its small displacement (Fig. 2) and the nature

of sediment exposed in the trenches, it is unlikely that the M_L 5.6 1950 surface break would be recognized in the absence of historical information in this setting. We cannot rule out the possibility that the fault has ruptured previously in multiple 1950-style events, but we can say that it does not characteristically rupture only in repeated, small-displacement 1950-style events. Instead, the fault has also produced less-frequent, much larger ruptures that are more typical of range-bounding Basin and Range normal faults. We do not observe a range in offsets between presumably more frequent 1950-type decimeter-scale ruptures and the rarer meter-scale surface offsets associated with paleoearthquakes P1 and P2. In this regard, the limited paleoseismic and historical evidence does not support either a strictly Gutenberg–Richter or characteristic earthquake model.

The reason for the variable surface-rupture behavior of the Fort Sage fault is not known, but a complicating factor is that this fault may at times break in conjunction with ruptures on nearby large strike-slip faults and thus may transfer slip between these larger structures (e.g. Caskey *et al.*, 1996). For example, paleoearthquakes on the nearby Honey Lake fault zone (Fig. 1) occurred during the intervals 5.6–6.7 ka and 4.7–5.6 ka (Turner *et al.*, 2008). Either of these Honey Lake events might correspond to paleoearthquake P1 documented in the Fort Sage trenches, but the present resolution of the ages of these events does not allow us to confidently correlate events between these adjacent faults.

Data and Resources

OxCal calibration and modeling of radiocarbon dates used in this study are from Bronk Ramsey, C. (2007). OxCal Program, v. 4.0, Radiocarbon Accelerator Unit, University of Oxford, UK; https://c14.arch.ox.ac.uk/oxcal.html (last accessed October 2011).

Faults depicted on Figure 1 and discussed in the Introduction are from Machette, M. N., K. M. Haller, R. L. Dart, and S. B. Rhea (2003). Quaternary fault and fold database of the United States, U.S. Geol. Surv. Open-File Rept. 03-417; http://earthquake.usgs.gov/regional/qfaults/ (last accessed November 2011).

Photographs of the 1950 Fort Sage Fault rupture discussed in the text are from Steinbrugge, K. V. (1958). Karl V. Steinbrugge Collection, University of California, Berkeley; http://nisee.berkeley.edu/visual_resources/steinbrugge_collection.html (last accessed September 2011).

GMPE analyses were conducted using software downloaded from Open SHA http://www.opensha.org/ (last accessed September 2011).

Acknowledgments

Anthony Crone, Steve Personius, Ryan Gold, Senthil Kumar, and Andrew Barron assisted with fieldwork. Ted and Alan Ramelli graciously provided the surface rupture photos in Figure 2. Chris Wills kindly provided the aerial photo used in Figure 3 and discussed the insights he gained from mapping the fault. Kenneth Adams helped clarify the Lake Lahontan highstand elevation at the site. Radiocarbon analyses were carried out by the Center for Accelerator Mass Spectrometry (CAMS) at Lawrence Livermore National Laboratory. This work was supported by the external grants program of the National Earthquake Hazards Reduction Program (NEHRP). Thoughtful reviews by Ryan Gold, Anthony Crone, Mark Stirling, and Richard Koehler greatly improved the manuscript. Center for Neotectonic Studies Contribution #63.

References

Abrahamson, N., and W. Silva (2008). Summary of the Abrahamson and Silva NGA ground-motion relations, *Earthq. Spectra* **24,** 67–98.

Adams, K. D., and S. G. Wesnousky (1998). Shoreline processes and the age of the Lake Lahontan highstand in the Jessup embayment, Nevada, *Bull. Geol. Soc. Am* **110,** 1318–1332.

Anderson, J. G., and J. N. Brune (1999). Probabilistic seismic hazard analysis without the ergodic assumption, *Seismol. Res. Lett.* **70,** 19–28.

Anderson, J. G., J. N. Brune, G. Biasi, A. Anooshehpoor, and M. Purvance (2011). Workshop report: Applications of precarious rocks and related fragile geological features to U.S. National Hazard Maps, *Seismol. Res. Lett.* **82,** 431–441.

Anooshehpoor, A., and J. N. Brune (2002). Verification of precarious methodology using shake table tests of rocks and rock models, *Int. J. Soil Dynam. Earthq. Eng.* **22,** 917–922.

Balco, G., M. D. Purvance, and D. H. Rood (2011). Exposure dating of precariously balanced rocks, *Quaternary Geochronol.* **6,** 295–303.

Bell, J. W., J. N. Brune, T. Liu, M. Zreda, and J. C. Yount (1998). Dating precariously balanced rocks in seismically active parts of California and Nevada, *Geology* **26,** 495–498.

Biasi, G. P., and R. J. Weldon (2006). Estimating surface rupture length and magnitude of paleoearthquakes from point measurements of rupture displacement, *Bull. Geol. Soc. Am.* **96,** 1612–1623.

Boore, D. M., and G. M. Atkinson (2008). Ground-motion prediction equations for the average horizontal component of PGA, PGV, and 5%-damped PSA at spectral periods between 0.01 s and 10.0 s, *Earthq. Spectra* **24,** 99–138.

Bronk Ramsey, C. (2009). Bayesian analysis of radiocarbon dates, *Radiocarbon* **51,** 337–360.

Brune, J. N. (1996). Precariously balanced rocks and ground-motion maps for southern California, *Bull. Seismol. Soc. Am.* **86,** 43–54.

Brune, J. N. (2000). Precarious rock evidence for low ground shaking on the footwall of major normal faults, *Bull. Seismol. Soc. Am* **90,** 1107–1112.

Brune, J. N. (2003). Precarious rock evidence for low near-source accelerations for trans-tensional strike-slip earthquakes, *Phys. Earth Planet In.* **137,** 229–239.

Brune, J. N., and A. Anooshehpoor (1999). Dynamic geometrical effects on strong ground motion in a normal fault model, *J. Geophys. Res.* **104,** 809–815.

Brune, J. N., A. Anooshehpoor, M. D. Purvance, and R. J. Brune (2006). Band of precariously balanced rocks between the Elsinore and San Jacinto, California, fault zones: Constraints on ground motion for large earthquakes, *Geology* **34,** 137–140.

Campbell, K. W., and Y. Bozorgnia (2008). NGA ground motion model for the geometric mean horizontal component of PGA, PGV, PGD and 5% damped linear elastic response spectra for periods ranging from 0.01 to 10 s, *Earthq. Spectra* **24,** 139–171.

Caskey, S. J, S. G. Wesnousky, P. Zhang, and D. B. Slemmons (1996). Estimating prehistoric earthquake magnitude from point measurements of surface rupture, *Bull. Seismol. Soc. Am.* **86,** 761–787.

Chiou, B. S. J., and R. R. Youngs (2008). An NGA model for the average horizontal component of peak ground motion and response spectra, *Earthq. Spectra* **24,** 173–215.

Farr, T. G., P. A. Rosen, E. Caro, R. Crippen, R. Duren, S. Hensley, M. Kobrick, M. Paller, E. Rodriguez, L. Roth, D. Seal, S. Shaffer, J. Shimada, J. Umland, M. Werner, M. Oskin, D. Burbank, and D. Alsdorf (2007). The Shuttle radar topography mission, *Rev. Geophys.* **45,** RG2004, doi: 10.1029/2005RG000183.

Field, E. H., T. H. Jordan, and C. A. Cornell (2003). OpenSHA: A developing community-modeling environment for seismic hazard analysis, *Seismol. Res. Lett.* **74,** 406–419.

Gianella, V. P. (1957). Earthquake and faulting, Fort Sage Mountains, California, December, 1950, *Bull. Seismol. Soc. Am.* **47,** 173–177.

Granger, D. E., J. W. Kirchner, and R. Finkel (1996). Spatially average long-term erosion rates measured from in situ-produced cosmogenic nuclides in alluvial sediment, *J. Geol.* **104,** 249–257.

Hammond, W. C., and W. Thatcher (2007). Crustal deformation across the Sierra Nevada, northern Walker Lane, Basin and Range transition, western United States measured with GPS, 2000–2004, *J. Geophys. Res.* **112,** B05411, doi: 10.1029/2006JB004625.

Hemphill-Haley, M. A., and R. J. Weldon II (1999). Estimating prehistoric earthquake magnitude from point measurements of surface rupture, *Bull. Seismol. Soc. Am.* **89,** 1264–1279.

Kalkan, E., C. J. Wills, and D. M. Branum (2010). Seismic hazard mapping of California considering site effects, *Earthq. Spectra* **26,** 1039–1055.

Lienkaemper, J. J., and C. Bronk Ramsey (2009). Oxcal: Versatile tool for developing paleoearthquake chronologies—A primer, *Seismol. Res. Lett.* **80,** 431–434.

Linton, D. L. (1955). The problem with tors, *Geogr. J.* **121,** 420–487.

Ma, S., and G. C. Beroza (2008). Rupture dynamics on a bimaterial interface for dipping faults, *Bull. Seismol. Soc. Am.* **98,** 1642–1658.

Munguía, L., E. Glowacka, F. Suarez-Vidal, H. Lira-Herrera, and O. Sarychikhina (2009). Near-fault strong ground motions recorded during the Morelia normal-fault earthquakes of May 2006 in Mexicali Valley, B. C., Mexico, *Bull. Seismol. Soc. Am.* **99,** 1538–1551.

O'Connell, D. R. H., R. LaForge, and P. Liu (2007). Probabilistic ground-motion assessment of balanced rocks in the Mojave Desert, *Seismol. Res. Lett.* **78,** 649–662.

O'Connell, D. R. H., S. Ma, and R. J. Archuleta (2007). Influence of dip and velocity heterogeneity on reverse- and normal-faulting rupture dynamics and near-fault ground motions, *Bull. Seismol. Soc. Am.* **97,** 1970–1989.

Ogelsby, D. D., R. J. Archuleta, and S. B. Nielsen (1998). Earthquakes on dipping faults: The effects of broken symmetry, *Science* **280,** 1055–1059.

Pankow, K. L., and J. C. Pechmann (2004). The SEA99 ground-motion predictive relations for extensional tectonic regimes: Revisions and a new peak ground velocity relation, *Bull. Seismol. Soc. Am.* **94,** 341–348.

Petersen, M. D., A. D. Frankel, S. C. Harmsen, C. S. Mueller, K. M. Haller, R. L. Wheeler, R. L. Wesson, Y. Zeng, O. S. Boyd, D. M. Perkins, N. Luco, E. H. Field, C. J. Wills, and K. S. Rukstales (2008). Documentation of the 2008 update of the United States national seismic hazard maps, *Open-File Rept. U.S. Geol. Surv. 2008-1128*.

Power, M., B. Chiou, N. Abrahamson, Y. Yousef Bozorgnia, T. Shantz, and C. Roblee (2008). An overview of the NGA project, *Earthq. Spectra* **24,** 3–21.

Prescott, J. R., and J. T. Hutton (1994). Cosmic ray contributions to dose rates for luminescence and ESR dating: Large depths and long-term time variations, *Radiat. Meas.* **23,** 497–500.

Purvance, M. D., J. N. Brune, N. A. Abrahamson, and J. G. Anderson (2008). Consistency of precariously balanced rocks with probabilistic seismic hazard estimates in southern California, *Bull. Seismol. Soc. Am.* **98,** 2629–2640.

Reheis, M. (1999). Extent of Pleistocene lakes in the western Great Basin, *U.S. Geol. Surv. Misc. Field Studies Map MF-2323*, scale 1:800,000.

Reimer, P. J., M. G. L. Baillie, E. Bard, A. Bayliss, J. W. Beck, P. G. Blackwell, C. Bronk Ramsey, C. E. Buck, G. S. Burr, R. L. Edwards, M. Friedrich, P. M. Grootes, T. P. Guilderson, I. Hajdas, T. J. Heaton, A. G. Hogg, K. A. Hughen, K. F. Kaiser, B. Kromer, F. G. McCormac, S. W. Manning, R. W. Reimer, D. A. Richards, J. R. Southon, S. Talamo, C. S. M. Turney, J. van der Plicht, and C. E. Weyhenmeyer (2009). INTCAL 09 and MARINE09 radiocarbon age calibration curves, 0–50,000 years Cal BP, *Radiocarbon* **51,** 1111–1150.

Riebe, C. S., J. W. Kirchner, D. E. Granger, and R. C. Finkel (2000). Erosional equilibrium and disequilibrium in the Sierra Nevada, inferred from cosmogenic 26Al and 10Be in alluvial sediment, *Geology* **28,** 803–806.

Shi, B., A. Anooshehpoor, Y. Zeng, and J. N. Brune (1996). Rocking and overturning of precariously balanced rocks by earthquakes, *Bull. Seismol. Soc. Am.* **86,** 1364–1371.

Shi, B., Y. Zeng, and J. N. Brune (1997), Numerical simulations of earthquake ruptures: A comparison between thrust, normal, and contained strike-slip faulting, *Seismol. Res. Lett.* **68,** 333.

Spudich, P., W. B. Joyner, A. G. Lindh, D. M. Boore, B. M. Margaris, and J. B. Fletcher (1999). SEA99: A revised ground motion prediction relation for use in extensional tectonic regimes, *Bull. Seismol. Soc. Am.* **89,** 1156–1170.

Stirling, M. W., A. Anooshehpoor, J. N. Brune, G. Biasi, and S. G. Wesnousky (2002). Assessment of the site conditions of precarious rocks in the Mojave Desert, California, *Bull. Seismol. Soc. Am.* **92,** 2139–2144.

Stuiver, M., and H. A. Polach (1977). Discussion: Reporting of 14 C data, *Radiocarbon* **19,** no. 3, 355–363.

Thatcher, W., G. R. Foulger, B. R. Julian, J. Svarc, E. Quity, and G. W. Bawden (1999). Present day deformation across the Basin and Range Province, Western United States, *Science* **283,** 1714–1718.

Turner, R., R. Koehler, R. W. Briggs, and S. G. Wesnousky (2008). Paleoseismic and slip-rate observations along the Honey Lake fault zone, Northeastern California, USA, *Bull. Seismol. Soc. Am.* **98,** 1730–1736.

Wells, D. L., and K. J. Coppersmith (1994). New empirical relationships among magnitude, rupture length, rupture width, rupture area, and surface displacement, *Bull. Seismol. Soc. Am* **84,** 974–1002.

Wesnousky, S. G., A. D. Barron, R. W. Briggs, S. J. Caskey, S. Kumar, and L. Owen (2005). Paleoseismic transect across the northern Great Basin, USA, *J. Geophys. Res. B. Solid Earth Planets* **110,** B05408, doi: 10.1029/2004JB003283.

Wills, C. J. (1990). Honey Lake and related faults, Lassen County, Calif, *Div. Mines Geol, Fault Eval Rept, FER-214*, scale 1:24,000, 17 pp.

Appendix

OxCal Model

The following model was used in OxCal to generate the constraints on relative timing of paleoearthquakes P1 and P2 observed in the North and South trenches. Earthquakes are modeled as boundaries, OSL ages are entered as calendar ages BC, and uncertainties are two-sigma.

```
Plot()
{
Sequence("Fort_Sage_north_south_combined")
{
Boundary("base section");
//Footwall OSL dates, format is years BC, two sigma
C_Date("OSL-5", BC(30790),4380);
C_Date("OSL-4", BC(19590),3180);
// Paleoearthquake (P2)
Boundary("P2");
Phase("C2")
{
C_Date("OSL-2", BC(15890), 2660);
C_Date("OSL-3", BC(15890), 2240);
};
//Radiocarbon dates are max ages of paleoearthquake P1 from
North trench
R_date ("C2", 6250,100);
R_date ("C1", 5400,35);
```

```
// Paleoearthquake (P1)
Boundary("P1");
// OSL age from base of C1 colluvium in South trench
C_Date("OSL-1", BC(5750),1120);
// Boundary is 1950 historical earthquake
Boundary ("1950 Historical", 1950);
};
};
```

Geological Hazards Science Center
U.S. Geological Survey
Golden, Colorado 80401
(R.W.B.)

Center for Neotectonic Studies
University of Nevada, Reno
Reno, Nevada 89557
(S.G.W.)

Seismological Laboratory
University of Nevada, Reno
Reno, Nevada 89557
(J.N.B.)

Itasca Consulting Group
Minneapolis, Minnesota 55401
(M.D.P.)

Crustal Geophysics and Geochemistry Science Center
U.S. Geological Survey
Denver, Colorado 80225
(S.A.M.)

Manuscript received 10 November 2011